Dalton Transactions

ROYAL SOCIETY OF CHEMISTRY

PAPER

View Article Online
View Journal | View Issue

Cite this: *Dalton Trans.*, 2025, **54**, 11573

Synthesis of a xanthene-based macrocyclic imine ligand and two-step planarization by metalation with Ni^{2+} and Na^{+}†

Shigehisa Akine, *[a,b] Masato Nakano,[b] Yoko Sakata[a,b,c] and Seiji Tsuzuki[d]

Received 19th May 2025,
Accepted 7th July 2025

DOI: 10.1039/d5dt01183c

rsc.li/dalton

A xanthene-based macrocyclic π-containing imine ligand, H_4L^2, was newly designed and synthesized in order to obtain a series of metal-containing planar structures. Due to the xanthene framework with the methylene bridge, the macrocyclic molecule, H_4L^2, had a more planar structure than the corresponding diaryl-ether-type analogue, H_4L^1. This macrocyclic molecule, H_4L^2, was converted into the dinuclear nickel(II) complex, L^2Ni_2, which was characterized by spectroscopic techniques as well as crystallography. The planarity of the macrocyclic ligand, H_4L^2, was greatly improved by the introduction of two Ni^{2+} ions. Furthermore, the L^2Ni_2 molecule became more planar by incorporation of a Na^+ ion in the central O_6 binding cavity. Thus, the xanthene-based macrocycle, H_4L^2, allowed complexation with two different metal ions, Ni^{2+} and Na^+, to demonstrate a two-step improvement in the planarity.

Introduction

Compounds containing π-planes have attracted much attention as functional molecules based on their electronic and optical properties. The planarity of such π-containing molecules has a significant effect on their electronic and photophysical properties derived from the π-conjugation of the molecules. For example, various physicochemical properties, such as optical properties,[1] electrochemical properties,[2] efficiency of photovoltaics,[3] *etc.*, are influenced by the molecular planarity, which can be changed by introducing or changing the substituents.[4] The dynamic change in the molecular planarity can also cause a significant change in the fluorescent behavior.[5]

The planarity of some macrocyclic π-containing molecules can be easily controlled by the incorporation of guest species into the cavity, because the macrocyclic compounds generally show a good host–guest binding affinity. For example, the properties of porphyrin derivatives can be altered by protonation[6] and metalation[7] in the binding pocket, axial functionalization on the metal ions,[8] *etc.*, although the porphyrin derivatives are generally less flexible to allow a rather smaller conformational change. If a macrocyclic molecule has a larger cavity with two or more binding sites to accommodate multiple guest species, the planarity could be more drastically controlled, perhaps in a multistep manner by using two or more different types of guest species.

In this respect, the macrocyclic imine ligand, H_4L^1 (Scheme 1a (i)), which we have previously reported, exhibited a unique two-step planarity enhancement, because this molecule has two types of binding sites inside the macrocyclic structure containing six benzene rings, *i.e.*, two H_2saloph‡ coordination pockets doubly connected by diaryl ether linkages and one central O_6 binding site.[9–13] The structure of H_4L^1 in the absence of metal ions is far from flat, but when Ni^{2+} ions are introduced into the saloph sites of this molecule, the two square planar [Ni(saloph)] structures are formed to make the L^1Ni_2 macrocycle relatively more planar (Scheme 1b (i)).[9,10] However, this L^1Ni_2 is still significantly deviated from an ideal planar structure, although the parent [Ni(saloph)] motif is known to be highly planar.[14] Particularly, the two [Ni(saloph)] substructures in the L^1Ni_2 macrocycle are curved in opposite directions to each other mainly due to the steric hindrance of the *ortho* hydrogen atoms in the diaryl ether moieties (Scheme 1b (i)).

If these two neighboring *ortho* hydrogen atoms are replaced with a bridging methylene group to make a xanthene motif, the resultant macrocycle is expected to be more planar. This

---

[a] Nano Life Science Institute (WPI-NanoLSI), Kanazawa University, Kakuma-machi, Kanazawa 920-1192, Japan. E-mail: akine@se.kanazawa-u.ac.jp
[b] Graduate School of Natural Science and Technology, Kanazawa University, Kakuma-machi, Kanazawa 920-1192, Japan
[c] Graduate School of Engineering, Nagoya University, Furo-cho, Chikusa-ku, Nagoya 464-8603, Japan
[d] Department of Applied Physics, The University of Tokyo, 7-3-1 Hongo, Bunkyo-ku, Tokyo 113-8656, Japan

† Electronic supplementary information (ESI) available. CCDC 2448855–2448857. For ESI and crystallographic data in CIF or other electronic format see DOI: https://doi.org/10.1039/d5dt01183c

‡ H_2saloph = *N*,*N*′-disalicylidene-*o*-phenylenediamine.

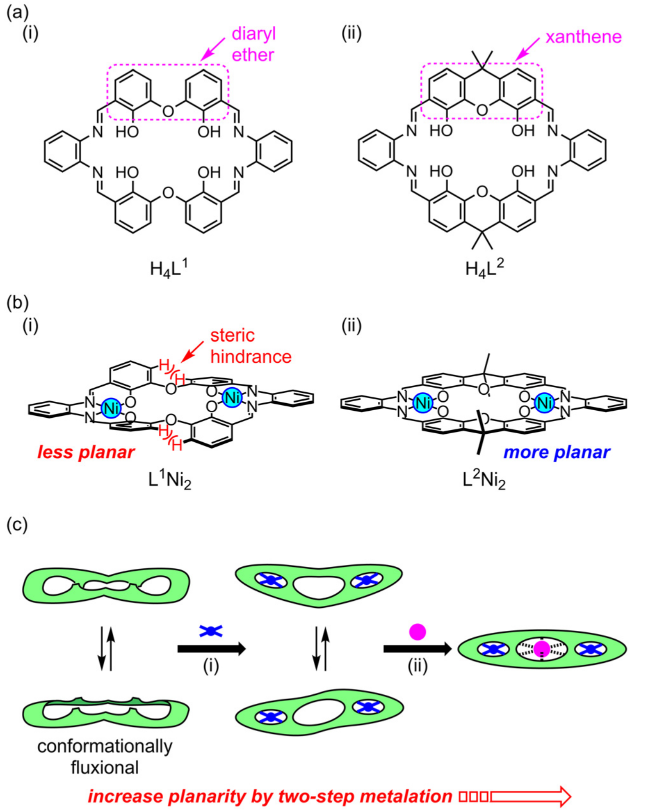

Scheme 1 (a) Molecular structures of bis(saloph) macrocycles: (i) diaryl-ether-based macrocycle H_4L^1 and (ii) xanthene-based macrocycle H_4L^2, and (b) their nickel(ɪɪ) complexes (i) L^1Ni_2 and (ii) L^2Ni_2. (c) Schematic drawing of two-step planarization of a macrocycle by metalation with two different kinds of metal ions, (i) the first metalation with Ni^{2+} and (ii) the second metalation with Na^+.

structural modification would lead to unique properties originating from the more effective π-conjugation and facilitate the formation of higher-order stacking structures.[9–11,15] In this study, we synthesized the macrocyclic imine ligand, H_4L^2, based on the xanthene motif (Scheme 1a (ii)), which can be converted into a planar dinickel(ɪɪ) complex, L^2Ni_2 (Scheme 1b (ii)). We found that the planarity of the macrocyclic ligand, H_4L^2, was greatly improved by introduction of two Ni^{2+} ions. Furthermore, the L^2Ni_2 molecule became more planar by incorporation of Na^+ ion into the O_6 binding cavity, demonstrating a two-step improvement in the planarity (Scheme 1c).

Results and discussion

Synthesis

For the synthesis of the precursor **4** for the macrocyclic ligand, H_4L^2 (Scheme 2), we first prepared 9,9-dimethylxanthene-4,5-diol (**1**) from xanthone according to a literature method.[16] The MOM protection of the hydroxy groups in this diol **1** gave the MOM ether **2** (Fig. S1, and S2†), which was then converted to dialdehyde **3** (Fig. S3, and S4†) by dilithiation followed by the reaction with DMF. Removal of the MOM groups by acid hydrolysis gave the dialdehyde **4** (Fig. S5, and S6†).

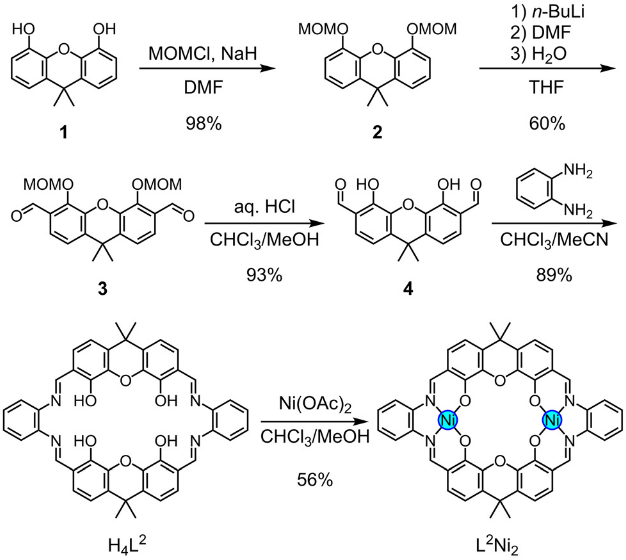

Scheme 2 Synthesis of xanthene-based macrocyclic ligand H_4L^2 and the corresponding metallohost L^2Ni_2.

The [2 + 2] macrocyclization of the dialdehyde **4** with *o*-phenylenediamine readily proceeded in a chloroform/acetonitrile (1 : 1) mixed solvent (Scheme 2). The macrocyclic ligand, H_4L^2, was obtained in 89% yield as orange crystals (Fig. S7–S11†). The product showed one singlet each for the imine proton at 8.99 ppm and the hydroxy proton at 13.82 ppm, indicative of the formation of a symmetric macrocyclic molecule. The mass spectrum showing *m*/*z* = 741.3 for $[H_4L^2 + H]^+$ confirmed the [2 + 2] macrocyclic structure of H_4L^2 (Fig. S12†). This compound was almost insoluble in pure chloroform or acetonitrile, while slightly soluble in DMSO.

The reaction of H_4L^2 with nickel(ɪɪ) acetate in chloroform/methanol then afforded the dinuclear nickel(ɪɪ) metallohost, L^2Ni_2, in 56% yield (Scheme 2; Fig. S13†). This metallohost showed a very low solubility in common organic solvents, and only very slightly soluble in DMSO.

Crystallography and theoretical studies

The H_4L^2 macrocycle crystallized in the monoclinic system, space group $P2_1/m$, and the crystallographic analysis clearly demonstrated the [2 + 2] macrocyclic structure (Fig. 1a and b). The unit cell contains two crystallographically independent molecules having different conformations, which are referred to as H_4L^2-A and H_4L^2-B, hereafter. Both conformations are found to be nonplanar as seen in the diaryl ether analogue, H_4L^1,[9,10] which is presumably due to the repulsion of the oxygen lone pairs. The H_4L^2-A molecule has a crystallographicaly imposed mirror plane and adopted an approximate C_{2v} symmetry. The two xanthene planes are bent by 39.12(4) deg to the same side with respect to the O_6 mean plane of the macrocycle resulting in a V-shaped structure (Fig. 1a). The other molecule, H_4L^2-B, has a crystallographically imposed inversion

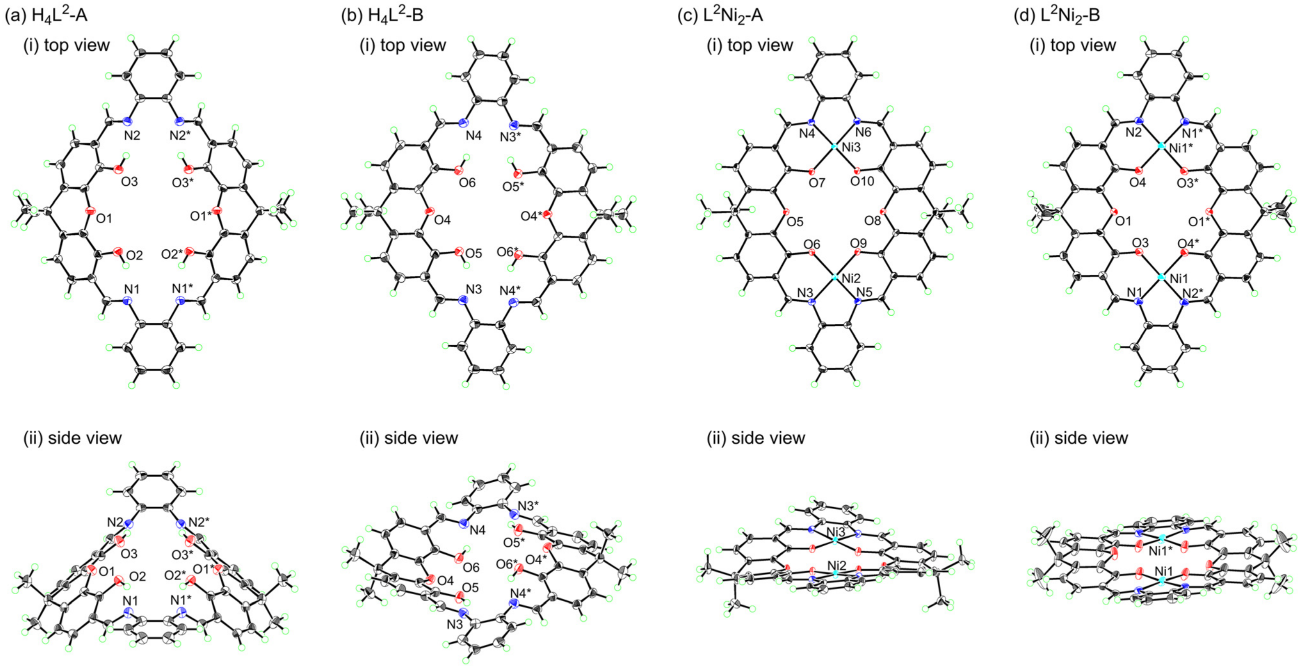
(a) H_4L^2-A (i) top view (ii) side view
(b) H_4L^2-B (i) top view (ii) side view
(c) L^2Ni_2-A (i) top view (ii) side view
(d) L^2Ni_2-B (i) top view (ii) side view

Fig. 1 X-ray crystal structures of H_4L^2 and L^2Ni_2 showing two crystallographically independent molecules. (a) H_4L^2-A with a V-shaped conformation; (b) H_4L^2-B with a step conformation; (c) L^2Ni_2-A with a shallow V-shaped conformation; (d) L^2Ni_2-B with a step conformation (ORTEP, 50% probability). Solvent molecules are not shown.

center and adopted an approximate C_{2h} symmetry. In contrast to molecule H_4L^2-A, the two xanthene planes are bent to the opposite side resulting in a step structure (Fig. 1b).

The relative stability of the two conformations of H_4L^2 was investigated by DFT calculations. The geometry optimizations were performed starting from the crystal structures, H_4L^2-A and H_4L^2-B, to obtain the corresponding optimized structures, H_4L^2-a and H_4L^2-b, respectively (Fig. S14†). The molecule of H_4L^2-a, which has a V-shaped structure, was more stable by 7.03 kJ mol^{-1} than H_4L^2-b having a step conformation.

In contrast to the metal-free macrocycle, H_4L^2, the corresponding nickel(II) complex has a more planar structure. The nickel(II) complex, L^2Ni_2, crystallized in the monoclinic system, space group $P2_1/n$, and the crystal structural analysis clearly demonstrated a macrocyclic structure containing two square planar nickel(II) ions in the saloph coordination pockets (Fig. 1c and d). The unit cell contains two crystallographically independent molecules, L^2Ni_2-A and L^2Ni_2-B hereafter, in a 2 : 1 ratio. The L^2Ni_2-A molecule had no crystallographically-imposed symmetry and was slightly bent to form a shallow V-shaped structure (Fig. 1c). The L^2Ni_2-B molecule had a crystallographically-imposed inversion center (Fig. 1d). The two xanthene moieties are slightly bent in the opposite directions to form a step-like conformation.

The geometry optimizations of L^2Ni_2 starting from the two structures, L^2Ni_2-A and L^2Ni_2-B, gave the corresponding energy-minimized structures, L^2Ni_2-a and L^2Ni_2-b, respectively, but both optimized structures were significantly curved unlike the nearly planar structures found in the crystalline state (Fig. S15†). L^2Ni_2-a is more stable than L^2Ni_2-b by only 2.97 kJ mol^{-1}, suggesting that both conformations as well as those in the crystalline state are present in the solution.

The macrocyclic metallohost, L^2Ni_2, was expected to show a binding affinity to cationic guest species, because it has a crown ether-like cavity. Indeed, the diaryl ether analog, L^1Ni_2, and related compounds showed an excellent binding affinity to alkali metal ions, *etc.*, mainly due to the more polarized phenoxo–Ni bonds.[9–11,17] In addition, Na^+ was the best metal to be accommodated in the binding cavity of L^1Ni_2 in a monomeric 1 : 1 stoichiometry. However, the guest binding behavior of L^2Ni_2 could not be investigated due to its very low solubility. Nevertheless, single crystals of the guest-inclusion complex, $[L^2Ni_2Na(DMSO)_2](OTf)$, was directly obtained by mixing H_4L^2, $Ni(OAc)_2$, and NaOTf in a methanol/DMSO solution followed by vapor-phase diffusion of diethyl ether.

The X-ray crystallographic analysis (Fig. 2) showed that a Na^+ ion was situated at the center of the O_6 cavity, exactly on the O_6 mean plane. The six Na–O distances are almost the same within a range of 2.531–2.665 Å, approximately forming a regular hexagon. This metallohost–guest complex, L^2Ni_2Na, adopted an almost planar but slightly wavy structure, and two DMSO molecules coordinated to the Na^+ ion from above and below the macrocyclic plane. In the packing structure, the planar [Ni(saloph)] substructures in this complex were stacked on top of each other in such a way that they avoided these coordinating DMSO molecules. The counter anion did not directly coordinate to any of the metal centers, Ni^{2+} or Na^+.

The DFT calculations gave the optimized structure of the inclusion complex, $[L^2Ni_2Na]^+$, with the coordinating DMSO molecules omitted (Fig. S16†). The calculated host–guest inter-

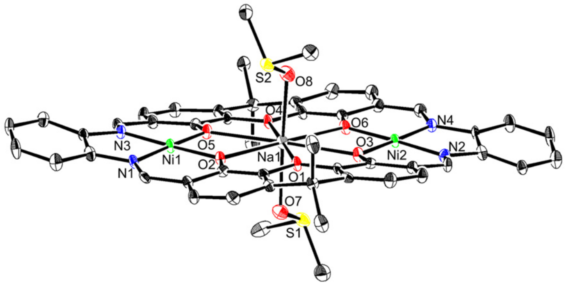

Fig. 2 X-ray crystal structure of $[L^2Ni_2Na(DMSO)_2]^+$ (ORTEP, 50% probability). Hydrogen atoms are omitted for clarity. Noncoordinating DMSO molecule and the TfO^- counter anion are not shown.

action energy between L^2Ni_2 and Na^+ using the optimized geometry was −528.5 kJ mol^{-1}. The destabilization by deformation of the L^2Ni_2 macrocycle caused by the formation of the Na^+ complex was calculated to be only 17.1 kJ mol^{-1}, indicating that the uncomplexed L^2Ni_2 already has a structure suitable for Na^+ binding. As a result, the stabilization energy upon the formation of $[L^2Ni_2Na]^+$ from L^2Ni_2 and Na^+ was determined to be −528.5 + 17.1 = −511.4 kJ mol^{-1}, which corresponds to the binding energy in the gas phase. In solution, the formation of $[L^2Ni_2Na]^+$ requires desolvation of Na^+; therefore, the binding energy in solution is expected to be much smaller (less negative). From the viewpoint of the small deformation energy associated with complex formation, along with favorable geometrical matching, this L^2Ni_2 macrocycle appears to be well preorganized for the Na^+ binding.

Planarity of the complexes

Since we have obtained the crystal structures of a series of H_4L^2, L^2Ni_2, and L^2Ni_2Na, their structural features, such as the planarity and cavities sizes/shapes, were summarized for comparison with the corresponding diaryl ether analogues (Table 1). Based on the X-ray crystal structures, we defined three parameters in order to discuss the planarity of the macrocyclic molecules; deviation d_{dev} as the average RMS deviation of the 40 skeletal carbon and 4 nitrogen atoms from the O_6 mean plane (Fig. 3a); macrocycle bent angle θ_a as the dihedral angle between the xanthene mean plane and the O_6 mean plane (Fig. 3b); and xanthene bent angle θ_b as the dihedral angle between the two benzene rings in each xanthene unit (Fig. 3c). In addition, the size/shape of the O_6 guest binding site is discussed in terms of the diagonal O⋯O distances, $d_{\mathrm{OO(X)}}$ and $d_{\mathrm{OO(P)}}$, as well as the continuous shape measure (CShM) value,[18] which represents the deviation from ideal regular hexagon.

As already mentioned, the metal-free macrocycles, H_4L^2-A and H_4L^2-B, have a non-planar conformation in which the two xanthene planes are bent at an angle θ_a of 37–39 deg with respect to the O_6 mean plane. The difference in the bending orientations of the two xanthene planes resulted in two types of conformations, *i.e.*, V-shaped (H_4L^2-A) and step-shaped (H_4L^2-B). In addition, each xanthene moiety was also bent at the angle θ_b of about 27–30 deg. This bending makes the molecular conformation far from planar, with the average deviation d_{dev} of 1.36 and 1.67 Å for H_4L^2-A and H_4L^2-B, respectively.

It was clear that the conversion of H_4L^2 into L^2Ni_2 by introducing two Ni^{2+} ions improved the overall planarity of the macrocyclic molecule; both molecules, L^2Ni_2-A and L^2Ni_2-B, showed the average deviations d_{dev} of 0.48–0.49, which are much smaller than those of H_4L^2. The nickel(II) complex, L^2Ni_2, also had bent angles θ_a (6.3–7.6 deg) and θ_b (12–23 deg) that are significantly smaller than those of H_4L^2. This planarization also changed the arrangement of the six oxygen atoms; in particular, the diagonal distance between the two xanthene oxygen atoms, $d_{\mathrm{OO(X)}}$, was shortened from 6.6 Å to 5.3 Å upon the conversion of H_4L^2 to L^2Ni_2. As a result, all the diagonal O⋯O distances within the O_6 binding site became almost similar ($d_{\mathrm{OO(P)}}$ of 5.05–5.15 Å), approximately making a regular hexagon, which is also evident from the significant decrease in the CShM values (from 3.2–3.5 to 0.2–0.7).

The incorporation of Na^+ ion into L^2Ni_2 further improved the planarity of the macrocycle. The deviation d_{dev} of $[L^2Ni_2Na(DMSO)_2](OTf)$ was 0.25, which was approximately half that for L^2Ni_2 (d_{dev} = 0.48–0.49). The bent angles θ_b became smaller

Table 1 Structural parameters for H_4L^2, L^2Ni_2, L^2Ni_2Na, H_4L^1, L^1Ni_2, and $L^{1'}Ni_2Na$

Structure	$d_{\mathrm{OO(X)}}$ [a] (Å)	$d_{\mathrm{OO(P)}}$ [b] (Å)	d_{dev} [c] (Å)	θ_a [d] (°)	θ_b [e] (°)	CShM [f]
H_4L^2-A	6.612(3)	5.683(2)	1.36	39.12(4)	27.28(10)	3.486
H_4L^2-B	6.597(3)	5.489(3), 5.865(3)	1.67	37.51(5)	30.41(10)	3.226
L^2Ni_2-A	5.261(12)	5.078(3), 5.151(3)	0.49	7.60(16)	12.64(12)	0.705
L^2Ni_2-B	5.3048(17)	5.0983(17), 5.0538(17)	0.48	6.38(5), 6.27(4)	23.21(9), 16.41(9)	0.221
L^2Ni_2Na [g]	5.319(4)	5.075(4), 5.077(4)	0.25	4.28(13), 5.86(13)	9.8(3), 7.6(3)	0.153
H_4L^1 [ref. 9 and 10]	6.354(2)	5.270(2), 5.956(2)	1.88	38.12(3), 75.28(4)	72.91(5)	4.624
L^1Ni_2 [ref. 9 and 10]	5.238(4)	5.167(4), 5.193(4)	0.80	29.29(11), 15.34(16)	42.24(13)	0.027
$L^{1'}Ni_2Na$-A [ref. 11] [h]	5.091(5)	5.070(5), 5.205(5)	0.82	25.41(11), 21.76(12)	44.46(10)	0.115
$L^{1'}Ni_2Na$-B [ref. 11] [h]	5.072(5)	5.189(5), 5.079(5)	0.85	22.60(13), 26.00(11)	45.66(10)	0.125

[a] The diagonal O⋯O distance between the xanthene oxygen atoms. [b] The diagonal O⋯O distance between the phenoxo oxygen atoms. [c] Average RMS deviation of the 40 skeletal carbon and 4 nitrogen atoms from the O_6 mean plane (Fig. 3a). [d] The dihedral angle between the xanthene mean plane and the macrocyclic O_6 mean plane (Fig. 3b). [e] The dihedral angle between the two benzene rings in each xanthene unit (Fig. 3c). [f] Continuous shape measure (CShM) value for the geometry calculated with the program SHAPE 2.1.[18] [g] $[L^2Ni_2Na(DMSO)_2](OTf)$. [h] $[L^{1'}Ni_2Na](OTf)$.

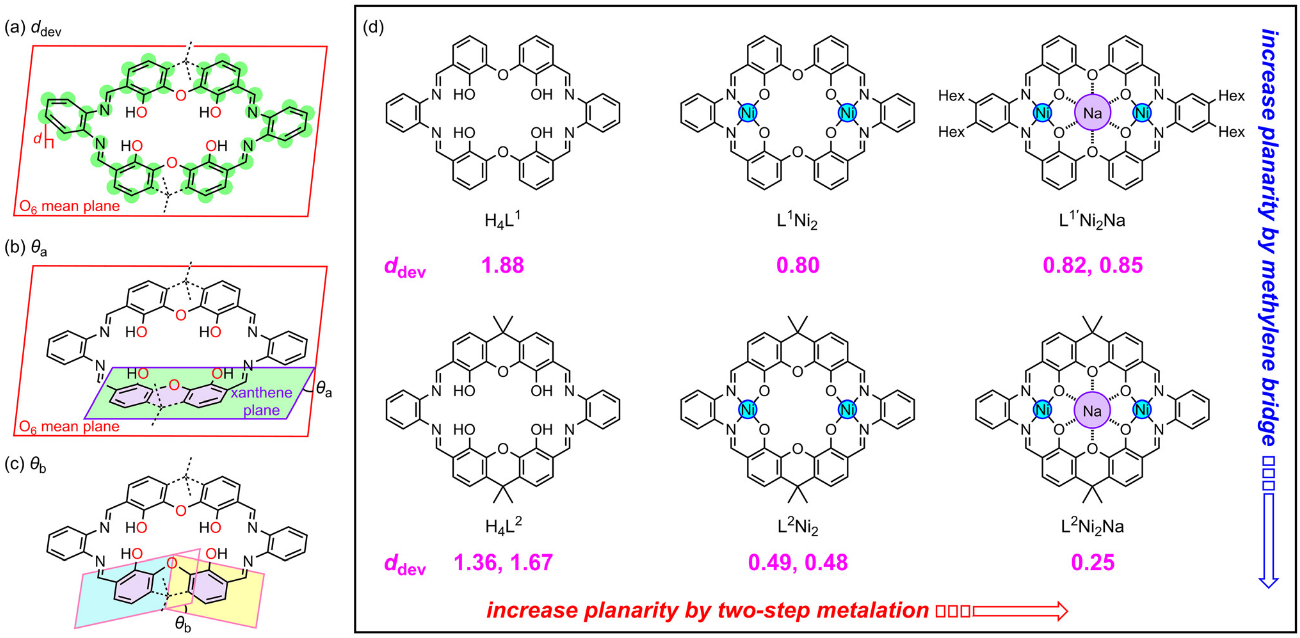

Fig. 3 Definition of planarity parameters (a) d_{dev}, (b) θ_a, and (c) θ_b. (d) Comparison of the planarity parameters for H_4L^1, L^1Ni_2, $L^{1'}Ni_2Na$, H_4L^2, L^2Ni_2, and L^2Ni_2Na.

(7.6–9.8 deg), which are also smaller than those of L^2Ni_2. Therefore, the planarity of this host H_4L^2 was clearly improved in two steps by introducing two different kinds of metals, Ni^{2+} and Na^+. Considering the molecular curvature found in the DFT calculated structures, the crystal packing may also contribute to the observed highly-planar structures of L^2Ni_2 and L^2Ni_2Na.

While there is a noticeable difference in the conformational planarity, the geometrical features of the O_6 sites of L^2Ni_2 and L^2Ni_2Na are quite similar. Whereas the CShM value for L^2Ni_2Na was slightly smaller than that for L^2Ni_2, it was particularly noteworthy that there is almost no difference in the diagonal O⋯O distances, $d_{OO(X)}$ and $d_{OO(P)}$, between the inclusion complex L^2Ni_2Na and the guest-free L^2Ni_2 macrocycle, indicating that Na^+ binding occurs almost without significant deformation of the host framework of L^2Ni_2. This was also demonstrated from the viewpoint of the deformation energy in the computational investigations as already discussed. Thus, the L^2Ni_2 metallohost has a well preorganized binding site that is particularly suitable for Na^+ binding.

A similar preorganization effect of the O_6 binding site was observed for the corresponding diaryl ether analogues, H_4L^1, L^1Ni_2,[9,10] and $L^{1'}Ni_2Na$.[11] However, the xanthene analogues presented here generally exhibit greater planarity than these diaryl ether analogues, particularly in the case of the metal-free H_4L^2. This enhanced planarity contributes to its stronger binding to Na^+ ($K_a = 182\ M^{-1}$; Fig. S17†) compared to H_4L^1 ($K_a = 13\ M^{-1}$),[9] owing to its well-preorganized binding site. Moreover, the xanthene analogues showed a more pronounced increase in planarity upon stepwise binding with Ni^{2+} and Na^+, demonstrating the advantage of employing the xanthene motif to construct metal-containing planar structures.

Conclusion

A novel xanthene-based macrocyclic imine ligand, H_4L^2, was designed and synthesized to make a planar metallohost molecule in which the aromatic organic macrocyclic moiety and the square planar metals are likely to form a coplanar structure. The use of the xanthene motif instead of the diaryl ether in H_4L^1 lead to a more planar structure of the resultant dinickel(II) metallohost without suffering the steric repulsion between the neighboring hydrogen atoms found in the diaryl ether analogues. From the viewpoint of the structural parameters, we demonstrated that the planarity of the H_4L^2 macrocycle was improved in a two-step manner by the introduction of Ni^{2+} into the H_2saloph coordination pockets followed by Na^+ in the O_6 guest binding site. Also, a detailed structural investigation clearly demonstrated that this L^2Ni_2 is well preorganized for the binding with Na^+ in the O_6 binding site. However, the present macrocycle, H_4L^2, and its nickel(II) complex, L^2Ni_2, showed a significantly low solubility in common organic solvents, which prevented us from investigating their behavior in solution. Nevertheless, the host–guest binding behavior and the possible formation of aggregated species would be of interest due to their highly-planar structures. Further investigations are currently underway to synthesize more soluble analogues by introducing alkyl groups into the phenylenediamine subunit, aiming to facilitate studies in solution chemistry.

Experimental section

General

9,9-Dimethylxanthene-4,5-diol was synthesized according to the literature.[16] The reagents and solvents were purchased from commercial sources and used without further purification. The ^{1}H and ^{13}C NMR spectra were recorded on a JEOL JNM-ECS 400 (^{1}H, 400 MHz; ^{13}C, 100 MHz) or a Bruker Avance 600 (^{1}H, 600 MHz). The chemical shifts were referenced with respect to tetramethylsilane (0 ppm) as an internal standard. The ESI-TOF mass spectra were recorded on a Bruker Daltonics micrOTOF II.

4,5-Bis(methoxymethoxy)-9,9-dimethylxanthene (2)

Under a nitrogen atmosphere, NaH (60% in oil, 5.63 g, 0.141 mol) was washed with petroleum ether to remove the oil and then a solution of 9,9-dimethylxanthene-4,5-diol (**1**) (8.72 g, 36.0 mmol) in dehydrated DMF (150 mL) was introduced into a flask containing the NaH. The resultant mixture was stirred for 4 h at rt, then chloromethyl methyl ether (8.20 mL, 0.108 mol) was added to the mixture at 0 °C, which was further stirred overnight at rt. After the addition of water, the mixture was extracted several times with chloroform. The combined organic layer was washed with brine, dried over anhydrous sodium sulfate, filtered, and concentrated to dryness under reduced pressure. The crude product was purified by column chromatography on silica gel (hexane/EtOAc, 9 : 1 → 4 : 1) to obtain MOM ether **2** (11.7 g, 35.3 mmol, 98%) as a pale yellow oil; ^{1}H NMR (400 MHz, $CDCl_3$) δ 1.62 (s, 6H), 3.57 (s, 6H), 5.30 (s, 4H), 7.00 (t, J = 7.8 Hz, 2H), 7.04 (dd, J = 7.8, 1.9 Hz, 2H), 7.09 (dd, J = 7.8, 1.9 Hz, 2H); ^{13}C NMR (100 MHz, $CDCl_3$) δ 31.81, 34.46, 56.30, 96.10, 115.78, 119.35, 122.77, 131.61, 141.49, 145.12. Anal. calcd for $C_{19}H_{22}O_5$: C, 69.07; H, 6.71. Found: C, 68.76; H, 6.69.

4,5-Bis(methoxymethoxy)-9,9-dimethylxanthene-3,6-dicarbaldehyde (3)

Under a nitrogen atmosphere, *n*-butyllithium (1.6 M in hexane, 6.0 mL, 9.6 mmol) was added to a solution of **2** (0.994 g, 3.01 mmol) in dehydrated THF (20 mL) at 0 °C. After the mixture was stirred for 1 h at 0 °C, dehydrated DMF (1.20 mL, 15.5 mmol) was added at 0 °C to the mixture, which was further stirred overnight at rt. After the addition of diluted hydrochloric acid (1.0 M, 20 mL), the mixture was extracted several times with chloroform. The combined organic layer was washed with brine, dried over anhydrous sodium sulfate, filtered, and concentrated to dryness under reduced pressure. The crude product was purified by column chromatography on silica gel (hexane/EtOAc, 9 : 1 → 4 : 1) to obtain dialdehyde **3** (0.692 g, 1.79 mmol, 60%) as pale yellow crystals; ^{1}H NMR (400 MHz, $CDCl_3$) δ 1.67 (s, 6H), 3.64 (s, 6H), 5.41 (s, 4H), 7.29 (dd, J = 8.4, 0.7 Hz, 2H), 7.62 (d, J = 8.4 Hz, 2H), 10.44 (d, J = 0.7 Hz, 2H); ^{13}C NMR (100 MHz, $CDCl_3$) δ 31.36, 35.65, 58.20, 100.08, 121.38, 122.27, 128.97, 137.33, 143.02, 147.96, 189.40. Anal. calcd for $C_{21}H_{22}O_7$: C, 65.28; H, 5.74. Found: C, 65.01; H, 5.75.

4,5-Dihydroxy-9,9-dimethylxanthene-3,6-dicarbaldehyde (4)

Hydrochloric acid (4.0 M, 9.0 mL) was added to a solution of **3** (2.25 g, 5.82 mmol) in methanol/chloroform (3 : 1, 48 mL) and the mixture was stirred overnight at rt. After the addition of water, the mixture was extracted with chloroform, and the combined organic layer was dried over anhydrous sodium sulfate, filtered, and concentrated under reduced pressure to a minimal volume. The addition of hexane to the resultant solution produced precipitates, which were collected on a filter to yield **4** (1.62 g, 5.43 mmol, 93%) as yellow crystals; ^{1}H NMR (400 MHz, $CDCl_3$) δ 1.67 (s, 6H), 7.06 (d, J = 8.4 Hz, 2H), 7.33 (d, J = 8.4 Hz, 2H), 9.91 (s, 2H), 11.21 (s, 2H); ^{13}C NMR (100 MHz, $CDCl_3$) δ 31.38, 35.62, 116.34, 119.52, 126.87, 136.81, 138.56, 150.33, 195.77. Anal. calcd for $C_{17}H_{14}O_5\cdot0.4H_2O$: C, 66.84; H, 4.88. Found: C, 66.86; H, 4.70.

Macrocyclic ligand H_4L^2

A solution of **4** (0.298 g, 1.00 mmol) in dehydrated chloroform (5 mL) was mixed with a solution of *o*-phenylenediamine (0.108 g, 1.00 mmol) in dehydrated acetonitrile (5 mL) and the resultant solution was allowed to stand for 2 d at rt. The reaction mixture was then filtered using a membrane filter and the filtrate was concentrated under reduced pressure to a minimal volume. The addition of hexane to the resultant solution gave precipitates, which were collected on a filter to yield H_4L^2 (0.365 g, 0.443 mmol, 89%) as orange crystals; ^{1}H NMR (400 MHz, DMSO-d_6) δ 1.64 (s, 12H), 7.17 (d, J = 8.4 Hz, 4H), 7.41 (d, J = 8.4 Hz, 4H), 7.46–7.50 (m, 4H), 7.56–7.60 (m, 4H), 8.99 (s, 4H), 13.82 (s, 4H); ^{13}C NMR (100 MHz, DMSO-d_6) δ 31.48, 34.93, 115.76, 117.68, 119.65, 126.74, 128.39, 133.93, 138.03, 141.82, 149.70, 164.56. ESI-TOF MS observed m/z = 741.2737 ($[H_4L^2 + H]^+$), calcd for $C_{46}H_{36}N_4O_6H$ m/z = 741.2713. Anal. calcd for $C_{46}H_{36}N_4O_6\cdot0.7CHCl_3$: C, 68.04; H, 4.49, N, 6.80. Found: C, 67.82; H, 4.78, N, 6.82.

Macrocyclic metallohost L^2Ni_2

A solution of H_4L^2 (21.0 mg, 28.3 μmol) in chloroform/methanol (1 : 1, 4 mL) was mixed with a solution of nickel(II) acetate tetrahydrate (21.1 mg, 84.8 μmol) in methanol (1.5 mL). After stirring for 6 h at rt, the resultant precipitates were collected on a filter to yield L^2Ni_2 (14.6 mg, 15.9 μmol, 56%) as brown crystals; ^{1}H NMR (400 MHz, DMSO-d_6) δ 1.61 (s, 12H), 6.88 (d, J = 8.6 Hz, 4H), 7.33–7.38 (m, 4H), 7.40 (d, J = 8.6 Hz, 4H), 8.15–8.19 (m, 4H), 8.85 (s, 4H). Anal. calcd for $C_{46}H_{32}N_4O_6Ni_2\cdot3.5H_2O$: C, 60.24; H, 4.29, N, 6.11. Found: C, 60.26; H, 4.14, N, 6.16.

X-ray crystallography

The intensity data were collected at 93 K on a Rigaku Mercury diffractometer (Mo Kα, λ = 0.71073 Å) or a Bruker APEX diffractometer (Cu Kα, λ = 1.54178 Å). The data were corrected for Lorentz and polarization factors, and for absorption by using semiempirical methods based on symmetry-equivalent and repeated reflections. The structures were solved by direct methods (SHELXS 97 or SIR 97)[19] and refined by full-matrix least-squares on F^2 using SHELXL 2014.[20] The crystallographic data are summarized in Table 2.

Computational methods

The Gaussian 16 program[21] was used for the DFT calculations. Geometries of the ligand (H_4L^2) and the metal complexes

Table 2 Crystallographic data

Formula	$H_4L^2·0.5CHCl_3·2.5MeCN$ $C_{51.5}H_{44}Cl_{1.5}N_{6.5}O_6$	$L^2Ni_2·0.67H_2O·0.67MeOH·1.33DMSO$ $C_{49.33}H_{44}N_4Ni_2O_{8.67}S_{1.33}$	$[L^2Ni_2Na(DMSO)_2](OTf)·DMSO$ $C_{53}H_{50}F_3N_4NaNi_2O_{12}S_4$
Formula weight	903.10	991.72	1260.62
Crystal system	Monoclinic	Monoclinic	Monoclinic
Space group	$P2_1/m$	$P2_1/n$	Pn
a (Å)	10.9940(14)	16.3754(5)	10.7194(4)
b (Å)	23.218(3)	21.6479(6)	9.1083(3)
c (Å)	17.421(3)	19.6275(6)	26.4196(9)
α (°)	90	90	90
β (°)	99.151(4)	111.4120(10)	99.796(2)
γ (°)	90	90	90
V (Å^3)	4390.2(10)	6477.6(3)	2541.88(15)
Z	4	6	2
D_{calcd} (g cm^{-3})	1.366	1.525	1.647
μ (mm^{-1})	0.178	2.217	3.239
Collected/unique reflections	41 360/7892	49 196/11 574	19 130/7753
$2\theta_{max}$	50.00	134.24	136.73
R_{int}	0.0460	0.0271	0.0484
Limiting indices	$-13 \le h \le 12$	$-19 \le h \le 19$	$-12 \le h \le 12$
	$-27 \le k \le 27$	$-23 \le k \le 25$	$-10 \le k \le 10$
	$-20 \le l \le 19$	$-23 \le l \le 23$	$-31 \le l \le 30$
Parameters/restraints	660/53	1044/277	796/136
GOF (F^2)	1.078	1.014	1.006
R_1 ($I > 2\sigma(I)$)[a]	0.0647	0.0334	0.0363
R_1 (all data)[a]	0.0749	0.0384	0.0472
wR_2 ($I > 2\sigma(I)$)[a]	0.1650	0.0854	0.0735
wR_2 (all data)[a]	0.1804	0.0886	0.0777
CCDC No.	2448855	2448856	2448857

[a] $R_1 = \sum||F_o| - |F_c||/|F_o|$; $wR_2 = \{\sum w(F_o^2 - F_c^2)^2/\sum[w(F_o^2)^2]\}^{1/2}$.

(L^2Ni_2 and $[L^2Ni_2Na]^+$) were optimized at the B3LYP/6-311G**[22] level with Grimme's D3 dispersion correction.[23] The relative energies of the different conformations were calculated at the same level using the optimized geometries. Interaction energies were calculated by the supermolecule method at the B3LYP/6-311G** level with Grimme's D3 dispersion correction. The basis set superposition error (BSSE)[24] was corrected by the counterpoise method.[25]

Conflicts of interest

There are no conflicts to declare.

Data availability

The data supporting this article have been included as part of the ESI.† Crystallographic data for $H_4L^2·0.5CHCl_3·2.5MeCN$, $L^2Ni_2·0.67H_2O·0.67MeOH·1.33DMSO$, and $[L^2Ni_2Na(DMSO)_2](OTf)·DMSO$ have been deposited at the CCDC under 2448855, 2448856, and 2448857† and can be obtained from **https://www.ccdc.cam.ac.uk/**.

Acknowledgements

We thank Dr Kenji Yoza (Bruker AXS) for the X-ray data collection of $L^2Ni_2·0.67H_2O·0.67MeOH·1.33DMSO$ and $[L^2Ni_2Na(DMSO)_2](OTf)·DMSO$. The research was partly supported by the Japan Society for the Promotion of Science (KAKENHI Grants JP21H05477 and JP23H04021 [Condensed Conjugation] as well as JP16H06510 [Coordination Asymmetry], JP18H03913, JP20K21206, JP23K17928 and JP23H01972) and the World Premier International Research Initiative, Ministry of Education, Culture, Sports, Science and Technology, Japan.

References

1 (*a*) M. Kivala and F. Diederich, *Acc. Chem. Res.*, 2009, **42**, 235–248; (*b*) J. A. Shelnutt, C. J. Medforth, M. D. Berber, K. M. Barkigia and K. M. Smith, *J. Am. Chem. Soc.*, 1991, **113**, 4077–4087; (*c*) N. I. Nijegorodov and W. S. Downey, *J. Phys. Chem.*, 1994, **98**, 5639–5643; (*d*) M. Kanematsu, P. Naumov, T. Kojima and S. Fukuzumi, *Chem. – Eur. J.*, 2011, **17**, 12372–12384; (*e*) F. Nifiatis, W. Su, J. E. Haley, J. E. Slagle and T. M. Cooper, *J. Phys. Chem. A*, 2011, **115**, 13764–13772.

2 (*a*) P. Frère and P. J. Skabara, *Chem. Soc. Rev.*, 2005, **34**, 69–98; (*b*) S. Maji and S. Sarkar, *Inorg. Chim. Acta*, 2010, **363**, 2778–2785.

3 (*a*) F. Zhang, R. Wang, Y. Wang, X. Zhanga and B. Liu, *Phys. Chem. Chem. Phys.*, 2019, **21**, 6256–6264; (*b*) Y. Liu, X. Zhang, C. Li, Y. Tian, F. Zhang, Y. Wang, W. Wu and B. Liu, *J. Phys. Chem. C*, 2019, **123**, 13531–13537.

4 (*a*) M. O. Senge, C. J. Medforth, T. P. Forsyth, D. A. Lee, M. M. Olmstead, W. Jentzen, R. K. Pandey, J. A. Shelnutt

and K. M. Smith, *Inorg. Chem.*, 1997, **36**, 1149–1163; (*b*) J. L. Retsek, C. J. Medforth, D. J. Nurco, S. Gentemann, V. S. Chirvony, K. M. Smith and D. Holten, *J. Phys. Chem. B*, 2001, **105**, 6396–6411; (*c*) T. Chandra, B. J. Kraft, J. C. Huffman and J. M. Zaleski, *Inorg. Chem.*, 2003, **42**, 5158–5172; (*d*) P. Bhyrappa, M. Sankar and B. Varghese, *Inorg. Chem.*, 2006, **45**, 4136–4149; (*e*) A. Y. Lebedev, M. A. Filatov, A. V. Cheprakov and S. A. Vinogradov, *J. Phys. Chem. A*, 2008, **112**, 7723–7733; (*f*) G. Conboy, H. J. Spencer, E. Angioni, A. L. Kanibolotsky, N. J. Findlay, S. J. Coles, C. Wilson, M. B. Pitak, C. Risko, V. Coropceanu, J.-L. Brédas and P. J. Skabara, *Mater. Horiz.*, 2016, **3**, 333–339; (*g*) Z. Zhang, M. Li, Y. Liu, J. Zhang, S. Feng, X. Xu, J. Song and Z. Bo, *J. Mater. Chem. A*, 2017, **5**, 7776–7783; (*h*) S. Kamiguchi, R. Akasaka, N. Yoshida, T. Imai, Y. Yamaoka, T. Amaya and T. Iwasawa, *Tetrahedron Lett.*, 2022, **92**, 153664.

5 (*a*) C. Yuan, S. Saito, C. Camacho, S. Irle, I. Hisaki and S. Yamaguchi, *J. Am. Chem. Soc.*, 2013, **135**, 8842–8845; (*b*) R. Kotani, H. Sotome, H. Okajima, S. Yokoyama, Y. Nakaike, A. Kashiwagi, C. Mori, Y. Nakada, S. Yamaguchi, A. Osuka, A. Sakamoto, H. Miyasaka and S. Saito, *J. Mater. Chem. C*, 2017, **5**, 5248–5256.

6 (*a*) S. Thyagarajan, T. Leiding, S. P. Årsköld, A. V. Cheprakov and S. A. Vinogradov, *Inorg. Chem.*, 2010, **49**, 9909–9920; (*b*) M. Ballester, L. Ravotto, J. M. E. Quirke, R. L. de la Vega, J. A. Shelnutt, A. V. Cheprakov, S. A. Vinogradov and C. J. Medforth, *J. Phys. Chem. A*, 2020, **124**, 8994–9003.

7 (*a*) Z. Valicsek and O. Horváth, *Microchem. J.*, 2013, **107**, 47–62; (*b*) M. Park, D.-G. Kang, H. Ko, M. Rim, D. T. Tran, S. Park, M. Kang, T.-W. Kim, N. Kim and K.-U. Jeong, *Mater. Horiz.*, 2020, **7**, 2635–2642.

8 B. A. Hussein, Z. Shakeel, A. T. Turley, A. N. Bismillah, K. M. Wolfstadt, J. E. Pia, M. Pilkington, P. R. McGonigal and M. J. Adler, *Inorg. Chem.*, 2020, **59**, 13533–13541.

9 S. Akine, F. Utsuno and T. Nabeshima, *Chem. Commun.*, 2010, **46**, 1029–1031.

10 S. Akine, F. Utsuno, S. Piao, H. Orita, S. Tsuzuki and T. Nabeshima, *Inorg. Chem.*, 2016, **55**, 810–821.

11 S. Akine, M. Nakano, Y. Sakata and S. Yano, *Chem. – Eur. J.*, 2024, **30**, e202403071.

12 (*a*) Y. Sakata, C. Murata and S. Akine, *Nat. Commun.*, 2017, **8**, 16005; (*b*) Y. Sakata, M. Tamiya, M. Okada and S. Akine, *J. Am. Chem. Soc.*, 2019, **141**, 15597–15604; (*c*) M. Cametti, Y. Sakata, J. Martí-Rujas and S. Akine, *Inorg. Chem.*, 2019, **58**, 14871–14875; (*d*) Y. Sakata, M. Okada, M. Tamiya and S. Akine, *Chem. – Eur. J.*, 2020, **26**, 7595–7601; (*e*) Y. Sakata, M. Okada and S. Akine, *Chem. – Eur. J.*, 2021, **27**, 2284–2288; (*f*) M. T. Chaudhry, B. O. Patrick, S. Akine and M. J. MacLachlan, *Org. Biomol. Chem.*, 2022, **20**, 8259–8268; (*g*) D. Walter, Y. Sakata and S. Akine, *Chem. – Asian J.*, 2025, **20**, e202401876.

13 Related macrocyclic bis(saloph) structures, see: (*a*) S. Akine, Z. Varadi and T. Nabeshima, *Eur. J. Inorg. Chem.*, 2013, 5987–5998; (*b*) Y. Sakata, S. Kobayashi and S. Akine, *Chem. Commun.*, 2017, **53**, 6363–6366; (*c*) Y. Sakata, S. Kobayashi, M. Yamamoto, K. Doken, M. Kamezawa, S. Yamaki and S. Akine, *Commun. Chem.*, 2024, 7, 166.

14 (*a*) A. Radha, M. Seshasayee, K. Ramalingam and G. Aravamudan, *Acta Crystallogr., Sect. C: Cryst. Struct. Commun.*, 1985, **41**, 1169–1171; (*b*) J. Wang, F.-L. Bei, X.-Y. Xu, X.-J. Yang and X. Wang, *J. Chem. Crystallogr.*, 2003, **33**, 845–849.

15 (*a*) A. J. Gallant and M. J. MacLachlan, *Angew. Chem., Int. Ed.*, 2003, **42**, 5307–5310; (*b*) S.-i. Kawano, Y. Ishida and K. Tanaka, *J. Am. Chem. Soc.*, 2015, **137**, 2295–2302.

16 Y. Sato, R. Yamasaki and S. Saito, *Angew. Chem., Int. Ed.*, 2009, **48**, 504–507.

17 (*a*) S. Akine and T. Nabeshima, *Dalton Trans.*, 2009, 10395–10408; (*b*) S. Akine, *J. Inclusion Phenom. Macrocyclic Chem.*, 2012, **72**, 25–54; (*c*) S. Akine, Metal Complexes with Oligo (salen)-Type Ligands, in *The Chemistry of Metal Phenolates, Volume 2*, ed. J. Zabicky, Patai's Chemistry of Functional Groups, John Wiley and Sons Ltd, Chichester, 2018, ch. 4, pp. 153–194.

18 M. Llunell, D. Casanova, J. Cirera, P. Alemany and S. Alvarez, *SHAPE 2.1*, University of Barcelona, Barcelona, Spain, 2013.

19 (*a*) G. M. Sheldrick, *SHELXS 97. Program for Crystal Structure Solution*, University of Göttingen, Göttingen (Germany), 1997; (*b*) A. Altomare, M. C. Burla, M. Camalli, G. L. Cascarano, C. Giacovazzo, A. Guagliardi, A. G. G. Moliterni, G. Polidori and R. Spagna, *J. Appl. Crystallogr.*, 1999, **32**, 115–119.

20 G. M. Sheldrick, *Acta Crystallogr., Sect. C: Struct. Chem.*, 2015, **71**, 3–8.

21 M. J. Frisch, G. W. Trucks, H. B. Schlegel, G. E. Scuseria, M. A. Robb, J. R. Cheeseman, G. Scalmani, V. Barone, G. A. Petersson, H. Nakatsuji, X. Li, M. Caricato, A. V. Marenich, J. Bloino, B. G. Janesko, R. Gomperts, B. Mennucci, H. P. Hratchian, J. V. Ortiz, A. F. Izmaylov, J. L. Sonnenberg, D. Williams-Young, F. Ding, F. Lipparini, F. Egidi, J. Goings, B. Peng, A. Petrone, T. Henderson, D. Ranasinghe, V. G. Zakrzewski, J. Gao, N. Rega, G. Zheng, W. Liang, M. Hada, M. Ehara, K. Toyota, R. Fukuda, J. Hasegawa, M. Ishida, T. Nakajima, Y. Honda, O. Kitao, H. Nakai, T. Vreven, K. Throssell, J. A. Montgomery, Jr., J. E. Peralta, F. Ogliaro, M. J. Bearpark, J. J. Heyd, E. N. Brothers, K. N. Kudin, V. N. Staroverov, T. A. Keith, R. Kobayashi, J. Normand, K. Raghavachari, A. P. Rendell, J. C. Burant, S. S. Iyengar, J. Tomasi, M. Cossi, J. M. Millam, M. Klene, C. Adamo, R. Cammi, J. W. Ochterski, R. L. Martin, K. Morokuma, O. Farkas, J. B. Foresman and D. J. Fox, *Gaussian 16, Revision C.01*, Gaussian, Inc., Wallingford CT, 2016.

22 A. D. Becke, *J. Chem. Phys.*, 1993, **98**, 5648–5652.

23 S. Grimme, J. Antony, S. Ehrlich and H. Krieg, *J. Chem. Phys.*, 2010, **132**, 154104.

24 B. J. Ransil, *J. Chem. Phys.*, 1961, **34**, 2109–2118.

25 S. F. Boys and F. Bernardi, *Mol. Phys.*, 1970, **19**, 553–566.